PAPER

First-principles evaluation of the secondary electron yield (γ^{N}) from polyethylene surface

IOP Publishing Journal of Physics D: Applied Physics

J. Phys. D: Appl. Phys. **53** (2020) 175301 (10pp) https://doi.org/10.1088/1361-6463/ab6af5

First-principles evaluation of the secondary electron yield (γ^N) from polyethylene surface

Giacomo Buccella[1,4], Davide Ceresoli[2], Andrea Villa[3], Luca Barbieri[3] and Roberto Malgesini[3]

[1] Departement of Chemistry, Materials and Chemical Engineering 'G. Natta', Politecnico di Milano P.zza L. da Vinci 32-20133, Milan, Italy
[2] Consiglio Nazionale delle Ricerche, Istituto di Scienze e Tecnologie Chimiche (CNR-SCITEC), I-20133 Milan, Italy
[3] Research Energy System—RSE, Via Rubattino 54, Milan, Italy

E-mail: giacomo.buccella@polimi.it, davide.ceresoli@cnr.it, andrea.villa@rse-web.it, luca.barbieri@rse-web.it and roberto.malgesini@rse-web.it

Received 6 November 2019, revised 17 December 2019
Accepted for publication 13 January 2020
Published 19 February 2020

Abstract

We have performed first-principles calculations (DFT) to estimate the secondary emission yield (SEY) through Auger neutralization mechanism (γ^N) related to the impact of a series of ions on a polyethylene surface. We have considered many relevant ionic species, such as Ar^+, which is often used as a benchmark. Our main goal is to study dielectric surfaces but, to check the validity of our approach, we have also considered some metallic surfaces (Al, Cu, Cu:N, Cu:O and CuO) on which some more experimental data can be found. On the contrary, very few references are available regarding the Auger neutralization on insulating materials and, in particular, on polyethylene.

The SEY outcomes for metals have basically reproduced the experimental references. In particular, the same decrease in γ^N, which has been associated to a 'dirty' (gas-exposed) metal surface, was confirmed by calculations. Thus, the applicability of the method to plastic material was considered to give realistic results. The computed γ^N values associated to polyethylene are in the order of 10^{-1} for most of the ionic species here considered.

Moreover, we have observed that a few percentage points of variations of the surface energy levels predicted by DFT calculations, may cause, depending on the ion type, a substantial change of γ^N. Therefore a detailed sensitivity analysis has been included to address this problem. The results associated to metals have shown that γ^N variations are, for some types of ions, very sharp, while this variability is milder for a polyethylene surface.

Our calculations are fully compatible with the previous relevant literature and suggest that plastic materials are characterized by γ^N coefficients similar to those of metals only slightly smaller.

Keywords: secondary electron yield, polyethylene, first-principles calculations (DFT), Auger neutralization

(Some figures may appear in colour only in the online journal)

[4] Author to whom any correspondence should be addressed.

1. Introduction

This work reports the theoretical calculation of the secondary emission coefficient from a polyethylene surface through the Auger neutralization mechanism (γ^N) [1]. Moreover, we have investigated theoretically the secondary emission properties of metallic surfaces in order to support the reliability of the method applied to plastic materials. The γ^N coefficient has been estimated for the collision of 17 different types of cations on the two different types of walls considered.

Due to its low cost and suitable dielectric properties, polyethylene is a polymer employed especially in electrical power industry where it is used as an insulating material. Unfortunately, under thermal and electrical stresses it ages leading, in many cases, to an unpredictable failure of electrical components. In AC power supply systems the main aging phenomenon is the treeing [2, 3]: a series of small discharges takes place inside some cavities embedded in the polymeric bulk. The accumulation of damages caused by discharges lead to the formation of a cluster of channels (also known as treeing branches) through the polyethylene matrix. When these channels bridge the gap between the electrodes then the final failure of the insulating material occurs.

Each discharge is triggered by the release of a Schottky electron from the surface in a gaseous cavity, see [4]. If the electric field inside the void is strong enough, the electron will undergo an avalanche effect. The resulting discharge gives rise to the formation of ions, radicals and other reactive chemical species. These species attack the polymeric walls leading to a propagation of the treeing. The impact of ions with the walls of the cavity triggers the release of further electrons through the Auger effect thus sustaining the discharge activity. In spite of the large literature on this topic, the process of treeing evolution is still poorly understood and this leads to a great uncertainty when estimating the residual life of electrical components.

Simulation tools, based on the solution of a set of partial differential equations (PDEs), are now massively used to shed a light on the treeing, the aging of polyethylene and, more in general, the aging of all polymeric insulating materials. Firstly, these kinds of tools have been applied to study the evolution of discharges in air such as corona and Trichel phenomena [5, 6]. The interaction of plasma with polymeric surfaces was included to address dielectric barrier discharges (DBDs), see [7, 8]. Then also the discharges in internal voids embedded in a polymeric matrix were included, see [9–11]. These latter simulations share many aspects of the physics of the propagation of discharges through treeing channels although the geometries considered are rather simplified: in many cases the voids have a spherical shape.

These simulation tools require knowledge of a large set of physical parameters some of which are rather poorly known. The quality of these kinds of simulations is to some extent strongly linked to the uncertainty of these parameters and, among them, the secondary emission coefficient plays a key role. Until now, this parameter has mainly been fitted to match the experimental data. In many cases, it is estimated that, for a metallic surface, its value varies in the interval 0.001–0.01, see [6, 12]. At least these values make it possible to match the period of some Trichel pulse experiments. Unfortunately, little is known about the useful values of γ^N to be used for polymeric surfaces and this has motivated the authors to undertake a first study on this aspect.

To be more specific, in plasma simulations, the total γ is what really matters, i.e. the result of the sum of all the possible secondary emission mechanisms. These processes can be split into those generated by a kinetic emission mechanism, and those triggered by a potential emission mechanism. It is already known [1, 13] that for slow ions ($<$1 keV) colliding on a metallic surface, the kinetic mechanism is negligible. On the other hand, it is also known that for the ionic dielectric system MgO [14–17] the kinetic emission becomes important for energies in the order of 10–100 eV . To the best of authors' knowledge, there are still no references regarding the kinetic emission for plastic materials.

As regards the potential emission mechanism, electron ejection (Auger effect) might be triggered by ions (γ_i) or metastable species (γ_m). The treatment of excited states would require the use of a more expensive theory such as TD-DFT, and this is beyond the purposes of the present work. The ionic collision might cause an electron ejection through the Auger neutralization process (γ^N) or through the two-step Auger de-excitation mechanism (γ^D). In [1] it has been demonstrated that, for ions impinging on a metallic surface, γ^D is negligible compared to γ^N. Moreover, in [18] is explained how the two-stage mechanism requires a relatively numerous series of energetic conditions. Therefore Auger de-excitation occurs much less frequently than Auger neutralization.

In the present work, we want to follow the same approach used in the computational study by Cho *et al* [14], where the authors have focused on the calculation of γ^N. In the same work, they have dealt also with the kinetic emission mechanism from various MgO surfaces. On the contrary, the present work has focused only on the evaluation of γ^N. However, we will show in section 3 that, in this particular case, the kinetic emission can be disregarded.

Our theoretical study of secondary electron emission has started considering a metal surface, and that's because, for similar systems, this subject has a fairly rich literature to refer to [1, 13, 19, 20]. To the best of the authors' knowledge, the secondary emission properties of insulating metal oxides such as MgO have been largely studied both with an experimental [15, 21, 22] and a theoretical/computational approach [14, 18, 23, 24]. However, this is not valid for all polymeric materials.

In this work, an investigation on pure and defective or oxidized metal surfaces have been carried out. These latter results have provided some preliminary tests in order to ensure the validity of our approach. We have evaluated γ^N associated to the surfaces of Al (0 0 1), Cu (0 0 1), Cu:N, Cu:O and CuO (0 0 1). Aluminum and copper are two of the mostly used conductors in electrical devices, and this is one of the reasons why they have been considered. Our aim was to reproduce the trend and the order of magnitude reported in the review of experimental analysis in the work of Phelps *et al* [13].

In this work, we have evaluated SEY associated with the impact of the following ions: N^+, N_2^+, N_3^+, N_4^+, O^+, O_2^+,

O_4^+, NO^+, N_2O^+, NO_2^+, H^+, H_2^+, H_3^+, OH^+, H_2O^+, H_3O^+, Ar^+. These species (except for Ar^+) are some of the main chemically reactive species present during a discharge in air according to [25]. We acknowledge that many other chemical databases are available, such as those described in [26], however the one included in [25] is one of the most detailed in terms of ionic species. The noble gas ion Ar^+ has been included and taken as a benchmark, since it has been considered in relevant experimental and computational studies, see [13, 14, 27].

In a gas ions drift due to the electric field and their approach speed depends upon their mobility and the actual electric field on the surface. We have considered a rather large interval ranging from 10^{-3} MV m^{-1} to 10^2 MV m^{-1} which covers almost all the conceivable discharge conditions in electrical devices.

As outlined in [14], the estimation of γ^N requires only the evaluation of a couple of convolution integrals whose characteristics depend upon some parameters that are derivable from first-principles calculations using DFT. Nevertheless, the original formulation of [27] plans to consider a series of corrections of the main parameters. As it will be explained in detail in the following section, these modifications have been neglected. The same choice was made in the work by Cho *et al* [14].

Our analysis has been complemented by a sensitivity analysis consisting in small variations of the fundamental surface energy parameters determining γ^N. This allowed us to provide data which take into account possible intrinsic inaccuracies embedded in an electronic structure DFT calculation. In particular, we have seen that even really small variations can affect the value of γ^N to a large extent.

In the calculations associated to the metallic surfaces, our benchmark was mainly the ion Ar^+. This was done for reproducing, as close as possible, the experimental data of Cu-based systems. We basically obtained a good agreement with the results reported by Phelps *et al* [13]. Indeed we found a γ^N value in the order of 10^{-1} for clean metallic surfaces (Cu and Al) and an appreciable decrease (one order of magnitude) of γ^N when we have considered an oxidized surface (CuO).

The experimental results reported by Phelps *et al* [13] distinguish between emission provoked by metastable species (γ_m) and that cause by ions (γ_i), but not between γ^N and γ^D. However, the relative infrequency of two-stage events (see [1]) makes it possible to directly compare our results with those reported by Phelps [13].

Even though we found no experimental comparison of SEY for polyethylene, our result with the Ar^+ ion ($\gamma^N = 0.2204$) is, at least, comparable with Hagstrum's theoretical analysis performed considering Ge (1 1 1) [27] (reproduced by computational modelling in [28]) and the numerical results of [14, 23] for pure and defective MgO.

The structure of the paper is the following. The next section is dedicated to the description of the integrals for the estimation of γ^N and the computational setup for DFT simulations. Results are listed in section 3, while a critical review of the data obtained is included in section 4. Section 5 concludes the paper.

2. Methods

We have considered the polymer geometry shown in figure 2 which represents a realistic configuration of the interface between a polyethylene *lamella* and an amorphous phase or microscopic void [29, 30]. This system has adjacent polymeric chains connected by four methylenic units. This arrangement allows to maintain the continuity of chemical bonds, thus avoiding any formation of unsaturated centers or exposed methyl groups. Nevertheless, in the literature, several other arrangements have been considered. For instance, in [4] authors have performed DFT calculations on the (1 1 0) slab of polyethylene, reporting a band gap between 5.7 and 5.8 eV. The structure considered here presents a band gap equal to 5.83 eV, and the electronic structure is substantially unchanged between the various crystalline exposed faces.

As regards the *ab initio* modeling, we have used Quantum ESPRESSO, which is an integrated suite of computer codes for solid-state and electronic-structure calculations based on DFT, plane waves, and pseudopotentials [31]. We have performed calculations on slab systems of polyethylene, clean Al, Cu (both clean and with adsorbates) and pure CuO. We have extracted for each system the density of states (DOS) distribution $D(\varepsilon)$ and the Fermi energy ε_F by first performing a self consistent field (*scf*) calculation, then a *non−scf* calculation with an increased sampling of the reciprocal cell. The subsequent plotting led us to identify the energy position of the VB top (ε_v), VB bottom (for the sake of convenience shifted to 0) and CB bottom (ε_c). Next, we have extracted the map of the electrostatic potential energy averaged in the plane perpendicular to the c-axis (i.e. along the thickness of each slab). Vacuum level ε_0 is obtained as the energy corresponding to the flat plateau of the electrostatic potential in the vacuum region.

This energetic description is needed to implement and solve the integrals which appear in the definition of γ^N that we are going to introduce; see also [14, 18].

We point out that the resulting value of γ^N strongly depends on the ionization potential of the incoming ion E_i [1, 27, 32]. To be precise, this value is dependent on the fluctuations of the energy levels resulting from the approach of the ion towards the surface. This implies that the actual value of γ^N depends on the distance s of the ion from the surface. On the other hand, experimental observations demonstrated that the transition probability $P_t(s, v)$, where v is the approaching speed, reaches a maximum at $s = s_m$ [1, 18, 27]. Therefore, to model a good approximation of γ^N, one should know the value of s_m and from that calculate the related ionization potential E_i' to replace E_i. E_i' is defined as

$$E_i'(s) = E_i + E(i - surf) - E(n - surf), \qquad (1)$$

where $E(i - surf)$ and $E(n - surf)$ are the energies of interaction of the ion and the neutral species with the surface,

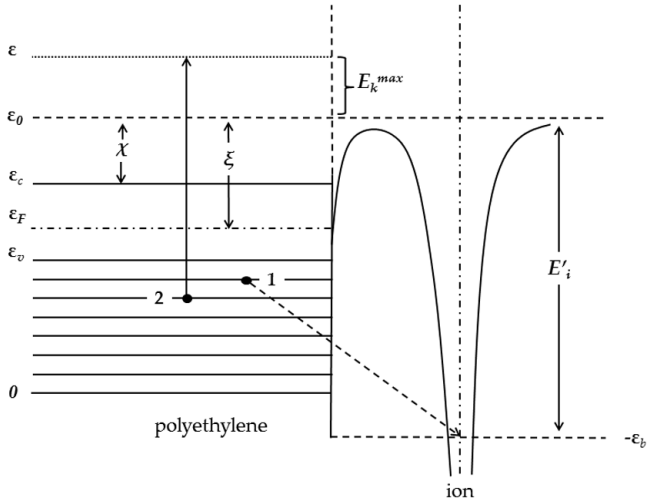

Figure 1. Diagram illustrating electronic transitions involved in the Auger neutralization mechanism at the polyethylene surface: an electron (1) neutralizes the incoming ion and another one (2) is ejected. ε is the electron energy, ε_0 is the vacuum, ε_c is the bottom of the conduction band, ε_F is the Fermi level, ε_v is the top of the valence band, ξ is the work function, χ is the electron affinity, E_k^{max} is the maximum kinetic energy of the ejected electron, E_i' is the effective ionization potential and $\varepsilon_b = E_i' - \varepsilon_0$.

as described in [1, 27]. However, in practical calculations, it is really difficult to know the exact value of s_m or even $E(i-surf)$ and $E(n-surf)$. For instance, Hagstrum obtained these quantities by fitting experimental data [27].

In the present work, we are mainly interested in reproducing at least the order of magnitude of experimental results of γ^N in metals, and then in applying a very similar strategy to polyethylene. For this reason, as it will be shown in section 3, we have chosen to calculate the ionization potentials of the species in vacuum. These were taken from the literature, as done by [14], or obtained with DFT calculations in vacuum. In the latter case, we have simply performed two *scf* cicles of the molecule isolated, once neutral and once ionized. The ionization potential has been obtained as: $E_i = E^{scf}(ion) - E^{scf}(neutral)$. The secondary emission coefficient can be computed as:

$$\gamma^N = \frac{\int_{max\{\varepsilon_b,\varepsilon_0\}}^{E_i-2\xi+\varepsilon_0} P_e(\varepsilon) D_c(\varepsilon) \times T\left[\frac{\varepsilon+\varepsilon_0-E_i}{2}\right] d\varepsilon}{\int_{max\{\varepsilon_b,\varepsilon_c\}}^{E_i-2\xi+\varepsilon_0} D_c(\varepsilon) \times T\left[\frac{\varepsilon+\varepsilon_0-E_i}{2}\right] d\varepsilon}. \quad (2)$$

For a detailed discussion of the theory, the reader can also refer to [33]. For the sake of convenience, here we have labeled $\varepsilon_b = E_i - \varepsilon_0$, i.e. the depth (energy distance) of the hole energy level from the bottom of the band, which has been taken as the zero of the scale. E_k^{max} represents the maximum kinetic energy with wich an electron could be ejected [14, 18] (refer also to figure 1). P_e is the 'escape probability' [27], defined as

$$P_e = \frac{1}{2}\left[1 - \left(\frac{\varepsilon_0}{\varepsilon}\right)^{\beta}\right]^{\alpha}. \quad (3)$$

This function defines the ejection probability dependent on the angle that the electron trajectory forms with the surface. The two parameters α and β are indeed adjustable coefficients that have been set equal to the reference values of $\alpha = 0.248$ and $\beta = 1.0$ according to some empirical observations associated to He^+ ions on a Ge surface; see [27]. Since these parameters are not well known for insulating materials, then we have also performed, in that case, a sensitivity analysis.

T is the Auger transform [1, 27, 34], and it is defined as:

$$T\left[\frac{\varepsilon+\varepsilon_0-E_i}{2}\right] = \int_0^{\varepsilon_v}\int_0^{\varepsilon_v} D_v(\varepsilon_1) D_v(\varepsilon_2) \times \delta(\varepsilon - \varepsilon_1 - \varepsilon_2 + \varepsilon_0 + E_i) d\varepsilon_1 d\varepsilon_2 \quad (4)$$

D_v and D_c are the DOS functions of the valence band and the conduction band, respectively. Once again, the rigorous application of the theory of Hagstrum would provide some corrections. T would have to be subject to the convolution with a broadening function, obtainable from the fitting of experimental data. However, this effect becomes more important when an ion approaches the surface with high kinetic energy. Moreover, D_v should be weighted with an appropriate function, which introduces a variation, depending on energy, of the transition probability through the valence band. This latter correction is necessary to have a discrimination against electrons s and p lying at the top of the band, which have different symmetry characteristics and different transition probabilities [27]. Also these corrections, according to Cho *et al* [14], have been neglected.

Definitions of γ^N and T are suitable for systems with energy gaps. Nevertheless, integrals can be adapted to be applied to a metallic system. This was done by simply replacing both ε_v and ε_c with ε_F. Redefining the limits of integration in this way, the distribution $D(\varepsilon)$, which for metals is continuous, is appropriately divided into populated and not populated portions.

2.1. PAW-DFT computational setup

Since the unit cells we have optimized were large, the derived reciprocal cells were small in volume. Therefore all the simulations were carried out by setting only one k-point in the Γ position of the Brillouin zone. Ultra-soft pseudo-potentials related to an Hamiltonian with PBE exchange-correlation functional, see [35], were employed throughout. For the polyethylene slab, the energy cut-off was set to 35 Ry, and the vacuum length of the optimized structure was 14.15 Å. For Al (0 0 1) the energy cut-off was set to 35 Ry with 17.5 Å of vacuum. For pure and defective Cu (0 0 1) slabs the cut-off was 40 Ry and the vacuum length 14.5 Å. In the case of the CuO (0 0 1) the cut-off was set to 35 Ry, with 20 Å of vacuum.

3. Results

In this section we present our results of the SEY calculation associated to the collision of several ions on both metallic and plastic surfaces. For many species, the ionization potentials have been derived from the literature. Nevertheless, for those species for which no references were found, i.e. N_3^+, N_4^+, O_4^+,

Table 1. γ^N for a clean Al (0 0 1) surface for different types of ions. • E_i experimental and ° E_i calculated.

Ion		E_i/eV	γ^N	γ^N min	γ^N avg	γ^N max
N^+	•	14.54	0.2221	0.1120	0.2109	0.2671
N_2^+	•	15.58	0.2228	0.1121	0.2117	0.2691
N_3^+	°	10.98	0.2137	0.1116	0.2015	0.2467
N_4^+	°	7.83	0.0000	0.0000	0.0000	0.0000
O^+	•	13.60	0.2212	0.1120	0.2100	0.2650
O_2^+	•	12.07	0.2179	0.1120	0.2068	0.2590
O_4^+	°	8.87	0.1157	0.0000	0.0889	0.1864
NO^+	•	9.26	0.1579	0.0000	0.1301	0.2010
N_2O^+	•	12.89	0.2202	0.1118	0.2089	0.2629
NO_2^+	•	6.88	0.0000	0.0000	0.0000	0.0000
H^+	•	13.61	0.2212	0.1119	0.2100	0.2651
H_2^+	•	15.41	0.2226	0.1121	0.2116	0.2688
H_3^+	°	8.68	0.0000	0.0000	0.0681	0.1770
OH^+	°	13.75	0.2213	0.1120	0.2101	0.2654
H_2O^+	•	13.76	0.2214	0.1120	0.2101	0.2655
H_3O^+	°	4.38	0.0000	0.0000	0.0000	0.0000
Ar^+	•	15.76	0.2229	0.1121	0.2119	0.2695

Table 2. γ^N for a clean Cu (0 0 1) surface for different types of ions. • E_i experimental and ° E_i calculated.

Ion		E_i/eV	γ^N	γ^N min	γ^N avg	γ^N max
N^+	•	14.54	0.1743	0.0000	0.1292	0.2101
N_2^+	•	15.58	0.1810	0.1448	0.1880	0.2379
N_3^+	°	10.98	0.0000	0.0000	0.0000	0.0000
N_4^+	°	7.83	0.0000	0.0000	0.0000	0.0000
O^+	•	13.60	0.0000	0.0000	0.0667	0.1737
O_2^+	•	12.07	0.0000	0.0000	0.0000	0.0000
O_4^+	°	8.87	0.0000	0.0000	0.0000	0.0000
NO^+	•	9.26	0.0000	0.0000	0.0000	0.0000
N_2O^+	•	12.89	0.0000	0.0000	0.0248	0.1374
NO_2^+	•	6.88	0.0000	0.0000	0.0000	0.0000
H^+	•	13.61	0.0000	0.0000	0.0672	0.1742
H_2^+	•	15.41	0.1767	0.1353	0.1832	0.2333
H_3^+	°	8.68	0.0000	0.0000	0.0000	0.0000
OH^+	°	13.75	0.0818	0.0000	0.0745	0.1805
H_2O^+	•	13.76	0.0896	0.0000	0.0752	0.1815
H_3O^+	°	4.38	0.0000	0.0000	0.0000	0.0000
Ar^+	•	15.76	0.1856	0.1549	0.1928	0.2427

Table 3. γ^N for a CuO surface surface for different types of ions. • E_i experimental and ° E_i calculated.

Ion		E_i/eV	γ^N	γ^N min	γ^N avg	γ^N max
N^+	•	14.54	0.0000	0.0000	0.0000	0.0000
N_2^+	•	15.58	0.0000	0.0000	0.0236	0.1394
N_3^+	°	10.98	0.0000	0.0000	0.0000	0.0000
N_4^+	°	7.83	0.0000	0.0000	0.0000	0.0000
O^+	•	13.60	0.0000	0.0000	0.0000	0.0000
O_2^+	•	12.07	0.0000	0.0000	0.0000	0.0000
O_4^+	°	8.87	0.0000	0.0000	0.0000	0.0000
NO^+	•	9.26	0.0000	0.0000	0.0000	0.0000
N_2O^+	•	12.89	0.0000	0.0000	0.0000	0.0000
NO_2^+	•	6.88	0.0000	0.0000	0.0000	0.0000
H^+	•	13.61	0.0000	0.0000	0.0000	0.0000
H_2^+	•	15.41	0.0000	0.0000	0.0180	0.1308
H_3^+	°	8.68	0.0000	0.0000	0.0000	0.0000
OH^+	°	13.75	0.0000	0.0000	0.0000	0.0000
H_2O^+	•	13.76	0.0000	0.0000	0.0000	0.0000
H_3O^+	°	4.38	0.0000	0.0000	0.0000	0.0000
Ar^+	•	15.76	0.0000	0.0000	0.0318	0.1440

H_3^+, OH^+, H_3O^+, this energy parameter was obtained through DFT calculations.

Since the energy parameters which, in the definition, determine the integration range in γ^N (such as ξ[5]) were obtained through DFT calculations, their numerical value may be affected by a certain degree of uncertainty. Moreover, since we have neglected the corrections mentioned in section 2, we have evaluated the integrals in (2) and (4) considering a variation of $\pm 10\%$ for the following parameters: $\xi, \varepsilon_0, \varepsilon_c, \varepsilon_v, \varepsilon_F$. The variations have been evenly spaced in a $\pm 10\%$ range, centred in our reference value[6]. The interval has been sampled by executing the code a statistically significant number of times, which in our case turned out to be 30. We have seen that a finer spacing does not lead to a strong variation of the results.

The results obtained from calculations on metallic surfaces are presented in section 3.1 (tables 1–4) while the results for polyethylene slab are reported in section 3.2 (tables 4–6).

3.1. Metallic surfaces

We have considered Al (0 0 1) as the first metallic surface system, the DOS is plotted in figure 3[7]. Table 1 shows the γ^N values associated with the ion database together with Ar^+, which has been considered the most significant benchmark to evaluate the performance of the model.

In order to reproduce as closely as possible the situation described in the experimental works [13], a second performance test has been performed on clean and 'dirty' (gas-exposed) Cu surfaces. Results of clean Cu are reported in figure 4 and table 2.

Moreover, the work by Phelps *et al* reports some outcomes associated with metallic surfaces exposed to gases like O_2 and N_2 which reported an appreciable decrease in SEY [13]. In order to check the model's ability to reproduce this behavior, we have performed the same calculation on a Cu system with a single oxygen or nitrogen atom adsorbed on the metal surface. Anyway, no significant difference in γ^N values has been observed. Therefore, we have decided to consider a more advanced oxidation degree, and a pure CuO system has

[5] The work function is defined as $\xi = \varepsilon_0 - \varepsilon_F$, and both these two levels have been obtained through DFT calculation.

[6] That is, the γ^N value obtained in the first instance by using the energetic description produced by our calculation.

[7] In this graph, and in all the DOS graphs reported in this paper, 0 have been set at the beginning of the energetic scale, that is the VB bottom.

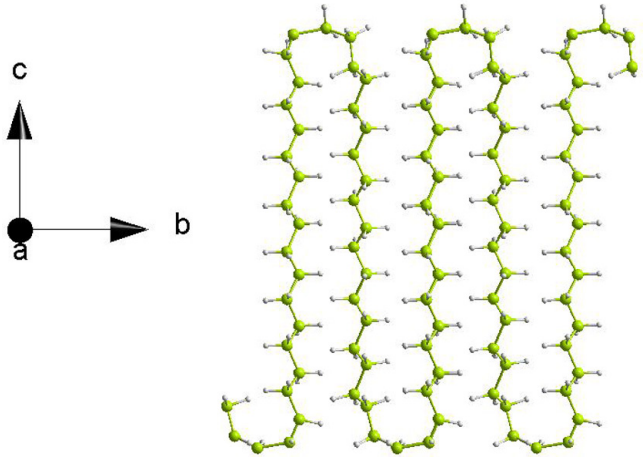

Figure 2. Polyethylene view along $\vec{a}$ direction.

been included in our calculations. The results are reported in figure 5 and table 3.

In this case the drop of the γ^N value is significant: the reference state is associated to a vanishing SEY while some small variations produce some non-zero γ^N.

3.2. Polyethylene surface

We have considered the conformation of the polymer described by Righi *et al* [30], which is represented in figure 2. In figure 6 we report the DOS diagram for both the bulk and the slab system of the polymer. From this graph it is possible to notice how the presence of surface states favors the narrowing of the energy gap. The states of the slab system around 15 eV are associated to the vacuum-exposed methylene groups, which link the polyethylene chains. The feature at around 20 eV is a diffused conduction state which springs from the formation of the surface/vacuum interface [36]. The results for γ^N on polyethylene are reported in tables 4–6.

In the first instance, we point out how a plastic material behaves similarly to metals. In fact, we have obtained values of γ^N in the order of 10^{-1} for most of the species considered. This was, to some extent, unexpected, due to the great difference, in terms of electronic transport, that exists between a metal and a plastic insulating material. Moreover, the sensitivity analysis with respect to the variations of the α (table 5) and β (table 12) parameters proves that slight variations of these coefficients do not imply any major variation of γ^N.

Unlike what Cho *et al* did [14], as has already been pointed out in section 1, the treatment of the electron emission derived from a kinetic mechanism has not been included in this work. Nevertheless, we have adopted a similar strategy to assess the emission probability through kinetic mechanism. That is, we have performed a first-principles molecular dynamics (FPMD) simulation, reproducing what we can consider as one of the most extreme (but also frequent) plasma conditions we are interested in (i.e. O_2^+ with an impact energy of ∼10 eV)[8]. At

[8] The estimated energy of ∼10 eV corresponds to the expected kinetic energy of an O_2^+ ion drifted by an electric field of 30 MV m^{-1}, which is associated to the dielectric strength of polyethylene.

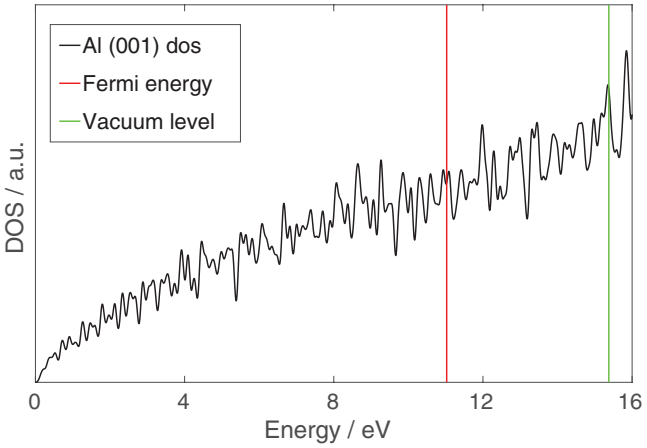

Figure 3. Density of states of the Al slab.

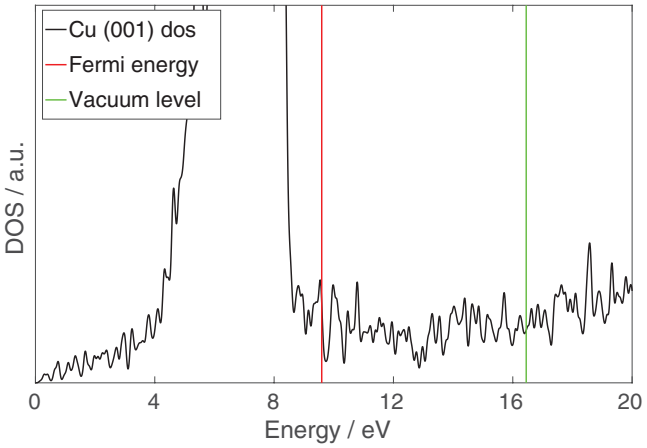

Figure 4. Density of states of the Cu (0 0 1) slab.

the beginning of the simulation the Fermi energy was 5.6 eV below the vacuum level, and during the dynamics (after the collision) it reached a maximum at 1.9 eV below the vacuum level. Unlike what was obtained by Cho *et al*, the Fermi energy of the entire system remains firmly below the vacuum level. Therefore, considering this result and the lack of any experimental reference which contradicts our findings, electron emission through kinetic mechanism can be disregarded.

4. Discussion

Regarding metal surfaces, we first consider the results of Al which is a relatively light metal, easy to computationally manage and often employed as a component in several electric devices such as high voltage power cables [37] and overhead lines [38]. Table 1 lists its SEY results corresponding to our complete ion database. Depending on the ionization energy, several different configurations may occur. If the potential energy of the ion is very low, then, even considering some variations of the surface energetic characteristics, the SEY vanishes. This is the case of N_4^+, NO_2^+ and H_3O^+. Then we have some boundary cases, such as the ones of O_4^+, NO^+, H_3^+, where the ionization is still too low to generate any secondary emission. However if we consider some variations of the energy levels produced by DFT electronic calculations,

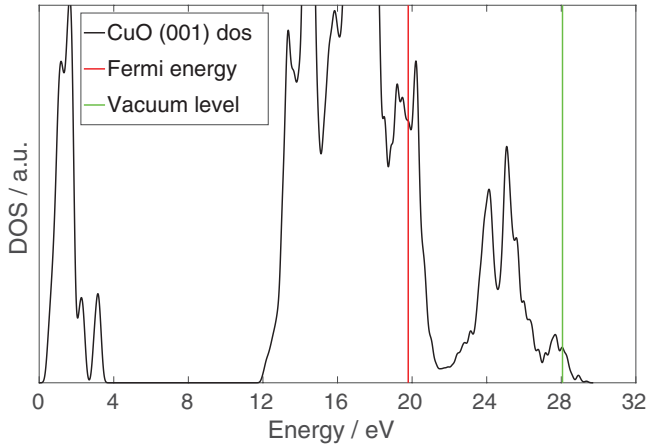

Figure 5. Density of states of the CuO slab.

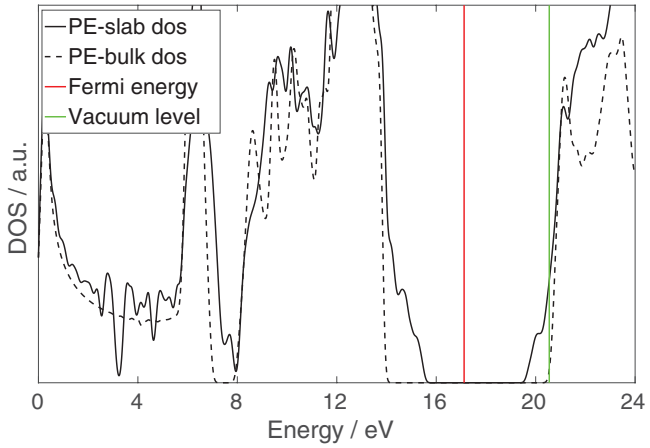

Figure 6. Density of states of polyethylene systems.

then we get some not-vanishing results in the upper end of the interval. The complementary case is the one for N_3^+, O^+, O_2^+, N_2O^+, H^+, OH^+ and H_2O^+ where the reference energy configuration leads to a not null γ^N but, if we consider the lower spectrum of the variations, we can still get some vanishing values. Finally, the ions characterized by large ionization potentials, such as N^+, N_2^+, H_2^+ and Ar^+, have, in all cases, not null SEY values.

We also point out that, in many cases, the SEY value is either zero or close to 10^{-1}. In other words, there are few intermediate values. This is due to the fact that γ^N is very dependent on the specific value of the Auger transformation (4). This is, in fact, a convolution integral:

$$T\left[\frac{\varepsilon+\varepsilon_0-E_i}{2}\right]=\int_0^{\varepsilon_v} D_v(\varepsilon_1)D_v(\varepsilon+\varepsilon_0+E_i-\varepsilon_1)d\varepsilon_1, \tag{5}$$

between two shifted functions. To be more precise the function (i.e. D_v) is the same. If the shift $\varepsilon+\varepsilon_0+E_i$ is small, then there is no overlap between the original and the shifted function which leads to a vanishing result. On the contrary, if the shift is large enough, then the two functions have a non-null overlap and $T\left[\frac{\varepsilon+\varepsilon_0-E_i}{2}\right]\neq 0$. In these cases γ^N is mainly controlled by P_e and the specific shape of the DOS of Al (see figure 3). This induces γ^N to rapidly saturate at values of 10^{-1}, as confirmed by [22].

Table 2 lists γ^N associated to an ideal Cu surface. In this case, only a few ions report an ejection probability different from zero. For ions that produce some non-vanishing emission results, such as H^+, O^+ and N_2O^+ the γ^N_{max} are close to 10^{-1}, which is comparable with the results already shown for Al. Once again, we have evidence of how the γ^N is very sensitive to the displacement, even minimal (at most $\pm 10\%$), of the energy levels of the surface system. From another point of view, these results are very different from the ones we got in the case of Al, where inert ions were only a minority. However, this can be explained by referring to the DOS function (see figures 3 and 4). The Cu system presents a state density plot typical of a transition metal, i.e. it has a strong band associated to *d*-electrons below the Fermi level and, at higher energies, a substantial flattening of the state density trend. On the other hand, the shape of the Al DOS presents a general trend that can be associated with the free electron gas distribution of energy $D(\varepsilon)=C\varepsilon^{1/2}$ [39].

Table 4. γ^N at polyethylene surface for different types of ions. • E_i experimental and ◦ E_i calculated.

Ion		E_i/eV	γ^N	γ^N min	γ^N avg	γ^N max
N^+	•	14.54	0.1861	0.0032	0.1683	0.3135
N_2^+	•	15.58	0.2157	0.0220	0.1892	0.3219
N_3^+	◦	10.98	0.0532	0.0000	0.1021	0.2809
N_4^+	◦	7.83	0.0000	0.0000	0.0000	0.0000
O^+	•	13.60	0.1575	0.0000	0.1503	0.3051
O_2^+	•	12.07	0.1026	0.0000	0.1228	0.2911
O_4^+	◦	8.87	0.0000	0.0000	0.0536	0.2436
NO^+	•	9.26	0.0000	0.0000	0.0630	0.2541
N_2O^+	•	12.89	0.1337	0.0000	0.1375	0.2985
NO_2^+	•	6.88	0.0000	0.0000	0.0000	0.0000
H^+	•	13.61	0.1578	0.0000	0.1505	0.3052
H_2^+	•	15.41	0.2112	0.0195	0.1858	0.3206
H_3^+	◦	8.68	0.0000	0.0000	0.0488	0.2357
OH^+	◦	13.75	0.1619	0.0000	0.1529	0.3064
H_2O^+	•	13.76	0.1625	0.0000	0.1532	0.3065
H_3O^+	◦	4.38	0.0000	0.0000	0.0000	0.0000
Ar^+	•	15.76	0.2204	0.0245	0.1929	0.3232

The simulation of a 'dirty' Cu slab has been considered in order to compare its trends with the experimental data reported in the work of Phelps *et al*, where some metal surfaces exposed to various gases, such as N_2 and O_2, have been considered. This treatment seems to affect the final SEY, in particular γ^N decreases by nearly one order of magnitude [13]. In order to reproduce this result in our computational work, a first attempt has been carried out with a Cu slab in presence of two kinds of adsorbates (O and N, respectively). The results, omitted here, do not lead to any substantial difference from the data produced by clean Cu system.

Therefore, we have considered the simulation of a system characterized by a marked increase of the oxydation degree, i.e. a slab of Cu (II) oxide. The idea was to reproduce the

Table 5. γ^N for a polyethylene surface: sensitivity associated with the α parameter variation. • E_i experimental and ° E_i calculated.

Ion		E_i/eV	γ^N	γ^N min	γ^N avg	γ^N max
N^+	•	14.54	0.1861	0.1720	0.1863	0.2015
N_2^+	•	15.58	0.2157	0.2006	0.2159	0.2320
N_3^+	°	10.98	0.0532	0.0477	0.0533	0.0594
N_4^+	°	7.83	0.0000	0.0000	0.0000	0.0000
O^+	•	13.60	0.1575	0.1447	0.1577	0.1714
O_2^+	•	12.07	0.1026	0.0934	0.128	0.1128
O_4^+	°	8.87	0.0000	0.0000	0.0000	0.0000
NO^+	•	9.26	0.0000	0.0000	0.0000	0.0000
N_2O^+	•	12.89	0.1337	0.1223	0.1339	0.1462
NO_2^+	•	6.88	0.0000	0.0000	0.0000	0.0000
H^+	•	13.61	0.1578	0.1450	0.1580	0.1718
H_2^+	•	15.41	0.2112	0.1962	0.2114	0.2274
H_3^+	°	8.68	0.0000	0.0000	0.0000	0.0000
OH^+	°	13.75	0.1619	0.1489	0.1621	0.1761
H_2O^+	•	13.76	0.1625	0.1495	0.1627	0.1768
H_3O^+	°	4.38	0.0000	0.0000	0.0000	0.0000
Ar^+	•	15.76	0.2204	0.2052	0.2206	0.2368

Table 6. γ^N at the polyethylene surface: sensitivity associated with the β parameter variation. • E_i experimental and ° E_i calculated.

Ion		E_i/eV	γ^N	γ^N min	γ^N avg	γ^N max
N^+	•	14.54	0.1861	0.1814	0.1860	0.1904
N_2^+	•	15.58	0.2157	0.2103	0.2157	0.2207
N_3^+	°	10.98	0.0532	0.0518	0.0532	0.0544
N_4^+	°	7.83	0.0000	0.0000	0.0000	0.0000
O^+	•	13.60	0.1575	0.1535	0.1574	0.1611
O_2^+	•	12.07	0.1026	0.1000	0.1026	0.1050
O_4^+	°	8.87	0.0000	0.0000	0.0000	0.0000
NO^+	•	9.26	0.0000	0.0000	0.0000	0.0000
N_2O^+	•	12.89	0.1337	0.1303	0.1337	0.1368
NO_2^+	•	6.88	0.0000	0.0000	0.0000	0.0000
H^+	•	13.61	0.1578	0.1538	0.1577	0.1615
H_2^+	•	15.41	0.2112	0.2059	0.2111	0.2161
H_3^+	°	8.68	0.0000	0.0000	0.0000	0.0000
OH^+	°	13.75	0.1619	0.1578	0.1618	0.1657
H_2O^+	•	13.76	0.1625	0.1584	0.1625	0.1663
H_3O^+	°	4.38	0.0000	0.0000	0.0000	0.0000
Ar^+	•	15.76	0.2204	0.2149	0.2203	0.2255

surface layer of oxide present in a real Cu system exposed to a normal atmosphere. The DOS plot of CuO is reported in figure 5, and the γ^N results are collected in table 3.

Comparing it with table 2, a drastic reduction in the secondary emission values associated with the impact of each ion has been observed. To be more precise, the reference values of γ^N (third column) vanish for all the types of ions. Although this is consistent with the trend we expected, these results probably under-estimate the actual value of SEY. As a matter of fact, the sensitivity analysis highlights that variations of a few percentage points in energy levels are sufficient to obtain a significant secondary emission. In other words, γ^N_{avg} and γ^N_{max} reported values are in the interval $10^{-2} - 10^{-1}$ for those ions with E_i above 15 eV (i.e. N_2^+, H_2^+ and Ar^+). In particular the γ^N_{avg} coefficient for Ar^+ is close to 10^{-2} and this is consistent with the experimental results associated to 'dirty' Cu in [13].

The SEY for plastic materials has been analyzed with a very similar strategy. In figure 6, the DOS of the bulk of polyethylene is superimposed to that of our slab system. γ^N have been obtained for all the ions previously mentioned. In addition to the sensitivity analysis associated to the variations of energy levels (table 4), in this phase we carried out a sensitivity study on both parameters α and β in equation (3). As mentioned above in section 2, the reference values ($\alpha = 0.248$ and $\beta = 1.0$) came out from a refinement of empirical data related to a Ge surface. For this reason, we have wanted to consider the possibility that, for a plastic material, these parameters might be slightly different. The results of the sensitivity study are reported in tables 5 and 6.

In table 4, the sensitivity results related to the variations of the energy levels have been reported. The nature of the material considered here, hugely different from that of metals, is clearly emphasized by these numbers: even though all γ^N other from zero are of the order of 10^{-1} (like for Al and Cu), the implementation of small variations revealed a weaker sensitivity. Those ions with $E_i \sim$ 8–9 eV and $\gamma^N = 0$, reported $\gamma^N_{avg} = 10^{-2}$ and $\gamma^N_{max} = 10^{-1}$. That is, in this case the fluctuations of the energy levels trigger some smoother modifications in γ^N. In general, we can state that a plastic surface gives a slightly lower γ^N than the simulated one for a clean metal. With several of the ions considered, the ejection probability for Auger neutralization is of the order of 10^{-1}. Nevertheless, really modest modifications in energy levels can cause a decrease to 10^{-2} or even fall to zero.

Just taking into consideration Ar^+, we obtained results comparable to the one published in [14] regarding MgO. These two materials are two different kinds of insulators, but the measured energy gaps are quite similar (7.8 eV for MgO [40] and 4.8 eV for polyethylene [41]). The energy gap represents a fundamental parameter to evaluate the material behavior in Auger processes. Therefore, we can state that the two insulators are quite comparable in these terms.

Let us now pass to describe the sensitivity analysis performed on the α and β parameters. These have been varied by $\pm 10\%$ and the results are displayed in tables 5 and 6 each reporting the sensitivity associated with each parameter separately. In this case the variations of γ^N are quite reduced. In other words, a slightly variation of the shape of the escaping probability P_e does not produce any significant effect.

5. Conclusions

Auger neutralization process, associated to both metals and plastic materials, has been trated with a computational approach. Preliminary calculations on clean, defective and oxidized metal surfaces have actually reproduced experimental observations. In particular, the same decrease in γ^N associated with gas-exposed surfaces reported by Phelps *et al*

[13] was confirmed by our calculations. Therefore, the applicability of the method to materials with different nature can be considered reliable.

Compared to the results obtained for metals, a similar strategy applied to plastic materials has originated slightly lower γ^N values, even though with a comparable order of magnitude. If we consider that the electronic transport in a plastic is noticeably different compared to that in a metallic system, these data are, to some extent, unexpected. Anyway, our results are consistent with other computational works on insulating materials [14, 23].

The sensitivity analysis on γ^N, especially for metals, reported some high values ($\sim 10^{-1}$) in all cases where the impacting ions have a large ionization potential. On the other hand, if E_i is not large enough SEY vanishes. Hence, in all other cases, γ^N strongly depends on both surface conditions and the accuracy of the description of the electronic levels involved, i.e. the DFT calculation. It is worth noting that even experimental data are quite scattered in a $10^{-1} - 10^{-2}$ range [13]. Anyway, polyethylene data reported a smaller sensitivity to energy levels variation: in some cases the γ^N magnitude is 10^{-2}.

To the best of author's knowledge, this is one of the first works devoted to Auger emission from plastic materials commonly used in electrical insulating systems. For some ions, our outcomes showed that SEY coefficients are much higher than the 0.001–0.01 range of values, which is currently used in the simulations of partial discharges in a gas [6, 12]. Therefore, a particular care must be taken as small variations of the composition of a given gas (for instance the humidity of air) may lead to a different composition of ions impacting surfaces and thus a different total secondary emission yield.

Acknowledgments

This work has been financed by the Research Found for the Italian Electrical System under the Contract Agreement between RSE and the Ministry of Economic Development.

The authors wish to thank L Barbareschi and M Trioni for their valuable contribution and suggestions.

ORCID iDs

Giacomo Buccella https://orcid.org/0000-0003-3080-6681
Davide Ceresoli https://orcid.org/0000-0002-9831-0773
Andrea Villa https://orcid.org/0000-0002-3282-945X
Luca Barbieri https://orcid.org/0000-0001-7296-9169
Roberto Malgesini https://orcid.org/0000-0002-9632-3829

References

[1] Hagstrum H D 1954 Theory of Auger ejections of electrons from metals by ions *Phys. Rev.* **96** 336–65
[2] Rowland S, Schurch R, Pattouras M and Li Q 2015 Application of FEA to image-based models of electrical trees with uniform conductivity *IEEE Trans. Dielectr. Electr. Insul.* **22** 1537–46
[3] Farr T, Vogelsang R and Frohlich K 2001 A new deterministic model for tree growth in polymers with barriers *Conf. on Electrical Insulation and Dielectric Phenomena, 2001 Annual Report* (https://doi.org/10.1109/CEIDP.2001.963625)
[4] Villa A, Leon-Garzon A R, Barbieri L and Malgesini R 2019 Ignition of discharges in macroscopic isolated voids and first electron availability *J. Appl. Phys.* **125** 043302
[5] Villa A, Barbieri L, Malgesini R and Leon-Garzon A R 2017 Simulation of the AC corona phenomenon with experimental validation *J. Phys. D: Appl. Phys.* **50** 435201
[6] Tran T N, Golosnoy I O, Lewin P L and Georghiou G E 2011 Numerical modelling of negative discharges in air with experimental validation *J. Phys. D: Appl. Phys.* **44** 015203
[7] Kang W S, Park J M, Kim Y and Houng S H 2003 Numerical study on the influence of barrier arrangements of dielectric barrier discharge characteristics *IEEE Trans. Plasma Sci.* **31** 504–10
[8] Serdyuk Y and Gubanski S 2005 Computer modeling of interaction of gas discharge plasma with solid dielectric barriers *IEEE Trans. Dielectr. Electr. Insul.* **12** 725–35
[9] Callender G, Golosnoy I, Lewin P L and Rapisarda P 2018 Critical analysis of partial discharge dynamics in air filled spherical voids *J. Phys. D: Appl. Phys.* **51** 125601
[10] Callender G, Tanmaneeprasert T and Lewin P L 2019 Simulating partial discharge activity in a cylindrical void using a model of plasma dynamics *J. Phys. D: Appl. Phys.* **52** 055206
[11] Villa A, Barbieri L, Gondola M, Leon-Garzon A R and Malgesini R 2017 A PDE-based partial discharge simulator *J. Comput. Phys.* **345** 687–705
[12] Binxian L, Hongyu S and Qiukun W 2017 Characteristics of Trichel pulse parameters in negative corona discharge *IEEE Trans. Plasma Sci.* **45** 2191–201
[13] Phelps A V and Petrović Z L 1999 Cold-cathode discharges and breakdown in argon surface and gas phase production of secondary electrons *Plasma Sources Sci. Technol.* **8** R21–34
[14] Cho Y, Kim C, Ahn H-S, Cho E, Kim T-E and Han S 2007 First-principles study on secondary electron emission of MgO surface *J. Appl. Phys.* **101** 083710
[15] Choi E-H, Lim J-Y, Kim Y-G, Ko J-J, Kim D-I, Lee C-W and Cho G-S 1999 Secondary electron emission coefficient of a MgO single crystal *J. Appl. Phys.* **86** 6525–7
[16] Riccardi P, Ishimoto M, Barone P and Baragiola R A 2004 Ion-induced electron emission from MgO by exciton decay into vacuum *Surf. Sci.* **571** 305–10
[17] Lee S, Kim J, Lee J and Whang K-W 2003 Secondary electron ejection from the MgO protection layer in AC plasma display panels for low-energy noble ions *Thin Solid Films* **435** 69–71
[18] Motoyama Y, Matsuzaki H and Murakami H 2001 A study and of the secondary and electron yield and of and insulator cathodes and for plasma and display panels *IEEE Trans. Ind. Appl.* **48** 1568–74
[19] Güntherschulze A 1930 Loss of electrons by collisions with positive ions at low gas pressures *Z. Phys.* **62** 600–6
[20] Rostagni A 1934 Ricerche sui raggi positivi e neutrali II—liberazione di elettroni da superfici metalliche *Nuovo Cimento* **11** 99–113
[21] Lim J Y, Oh J S, Ko B D, Cho J W, Kang S O, Cho G, Uhm H S and Choi E H 2003 Work function of MgO single crystals from ion-induced secondary electron emission coefficient *J. Appl. Phys.* **94** 764–9
[22] Chiang C-L, Zeng H-K, Li C-H, Li J-Y, Chen S-P, Lin Y-P, Hsieh T-C and Juang J-Y 2016 Secondary electron emission characteristics of oxide electrodes in flat electron emission lamp *AIP Adv.* **6** 015317

[23] Dai K, Tu Y, Yang L, Li Q and Tolner H 2014 First-principles study on secondary and electron emission and of MgO (2 0 0) and (1 1 1) surfaces *J. Soc. Inf. Disp.* **45** 212–4
[24] Uhm H S, Choi E H and Cho G S 2009 Secondary electron emission from MgO protective layer by Auger neutralization of ions *Appl. Phys. Lett.* **94** 031501
[25] Sakiyama Y, Graves D B, Chang H-W, Shimizu T and Morfill G E 2012 Plasma chemistry model of surface microdischarge in humid air and dynamics of reactive neutral species *J. Phys. D: Appl. Phys.* **45** 425201
[26] Komuro A, Ono R and Oda T 2013 Behaviour of OH radicals in an atmospheric-pressure streamer discharge studied by two-dimensional numerical simulation *J. Phys. D: Appl. Phys.* **46** 175206
[27] Hagstrum H D 1961 Theory of Auger and neutralization of ions and at the surface and of a and diamond-type semiconductor *Phys. Rev.* **122** 83–113
[28] Bercx M, Partoens B and Lamoen D 2019 Quantitative modeling of secondary electron emission from slow-ion bombardment on semiconductors *Phys. Rev.* B **99** 085413
[29] Dissado L A and Fothergill J C 1992 *Electrical Degradation and Breakdown in Polymers* (London: P. Peregrinus) ch 2
[30] Righi M C, Scandolo S, Serra S, Iarlori S, Tosatti E and Santoro G 2001 Surface states and negative electron affinity in polyethylene *Phys. Rev. Lett.* **87** 076802
[31] Giannozzi P *et al* 2009 Quantum ESPRESSO: a modular and open-source software project for quantum simulations of materials *J. Phys.: Condens. Matter* **21** 395502
[32] Hagstrum H D and D'Amico C 1960 Production and demonstration of atomically clean metal surfaces *J. Appl. Phys.* **31** 715–23
[33] Bonini N, Brivio G P and Trioni M I 2003 Theory of metastable deexcitation spectroscopy on simple metals *Phys. Rev.* B **68** 035408
[34] Lander J J 1953 Auger peaks and in the energy and spectra of secondary and electrons from various and materials *Phys. Rev.* **91** 1382–7
[35] Perdew J P, Burke K and Ernzerhof M 1996 Generalized gradient approximation made simple *Phys. Rev. Lett.* **77** 3865–8
[36] Teyssedre G and Laurent C 2005 Charge transport modeling in insulating polymers: from molecular to macroscopic scale *IEEE Trans. Dielectr. Electr. Insul.* **12** 857–75
[37] Jeroense M, Saltzer M and Ghorbani H 2014 Technical challenges linked to HVDC cable development *REE. Revue de l'électricité et de l'électronique*
[38] Straumann U and Franck C M 2013 Ion-flow field calculations of AC/DC hybrid transmission lines *IEEE Trans. Power Deliv.* **28** 294–302
[39] Ashcroft N W and Mermin N D 1976 *Solid State Physics* (New York: Cornell University)
[40] Taurian O E, Springborg M and Christensen N E 1985 Self-consistent electronic structures of MgO and SrO *Solid State Commun.* **55** 351–5
[41] Less K J and Wilson E G 1973 Intrinsic photoconduction and photoemission in polyethylene *J. Phys. C: Solid State Phys.* **6** 3110–20